Bias and bottlenecks study in outdoor long term thermal monitoring by infrared thermography: Leveraging opportunistic data for temperature estimation

Thibaud Toullier, Jean Dumoulin

Highlights

Bias and bottlenecks study in outdoor long term thermal monitoring by infrared thermography: leveraging opportunistic data for temperature estimation

T. Toullier, J. Dumoulin

- integration of opportunistic open data for environmental corrections on temperature estimation during long term thermal monitoring by infrared thermography
- Sensitivity study of measurement parameters (emissivity, sky temperature, atmospheric transmission, ..) over long time period for outdoor experiments

Bias and bottlenecks study in outdoor long term thermal monitoring by infrared thermography: leveraging opportunistic data for temperature estimation

T. Toullier[a], J. Dumoulin[a]

[a] *Université Gustave Eiffel, Inria, COSYS-SII, I4S Team, Bouguenais, F-44344, France*

Abstract

This study aims to assess the impact of the targeted scene and environmental variables on in situ long-term thermal monitoring by infrared thermography. It also addresses projection errors arising from camera perspectives and digitization. Over a span of 3 years, extensive measurements were conducted at two instrumented test sites, yielding a valuable dataset for analysis. The paper begins by introducing and discussing the model used to convert the collected data into surface temperature estimations and its associated parameters' sensitivities. Subsequently, it delves into the effects of camera resectioning on infrared measurements. Finally, the study investigates the influence of environmental parameters and proposes a strategy to correct for these effects, with and without additional sensors (opportunistic data) and additional in-situ measurements. Finally, a discussion is proposed and perspectives are addressed.

Keywords: thermography, calibration, emissivity, building, in-situ, copernicus, metar, open data

1. Introduction

Non-destructive thermal monitoring of transport infrastructures has become a major concern for next generations' civil engineering structures. In particular, SHM (Structural Health Monitoring) is of interest to estimate the influence of the thermal effect on modal analysis and correct it, as in [1] where a correlation between the temperature and the modal parameters

is shown, or in [2] where the potential use of online data to correct the environmental variation from the temperature variation is shown. Therefore, new long-term thermal monitoring solutions in situ, low cost, and robust are needed. If thermocouples or even optics fibers meet the expectation of thermal monitoring, their corresponding instrumentation may be complex with a risk of breaking during the construction (*i.e.* complex maintenance in operation). At the opposite, infrared thermography seems to be simpler to deploy and offers a potential temperature measurement on multiple points at the same time. Even if the technological context of uncooled infrared cameras is evolving quickly, methods and processes for using them as an accurate and low-cost alternative contactless and full field measurement system requires research efforts, in particular at ground based scale observations.

Numerous experiments have been conducted and examined in the literature to use infrared cameras in natural environments, for various applications. For instance, temperature estimation in natural environments such as [3] whose authors propose two intrusive references methods (aluminium mirror and temperature references), moisture detection as in [4], or even an application to detect the inner deck structure of a bridge in [5]. In [6], the authors propose the comparison of a numerical simulation of a radiative budget with an actual radiative measurement. However, these studies were either conducted under favorable environmental conditions and for a duration of not more than a few days, or used large computing and consuming resources that may not be suitable for every application. To advance understanding and capture real-world long-term data, specialized software architectures, such as C2IR, have been developed [7]. Thanks to this improvement of acquisition and computation means, instrumented multisensor test sites have gathered an interesting amount of synchronized and coupled data over the years.

The main challenge for using infrared cameras as a thermal monitoring tool is to convert the radiative fluxes received by the infrared camera to temperature. In fact, the underlying temperature estimation depends on many criterion such as camera calibration and internal parameters in operation[8, 9], geometrical considerations, but also environmental conditions. Therefore, to achieve quantitative thermography, one must consider the global radiative heat balance at the sensor level and be able to estimate the different parameters of the equation. In particular, meteorological varying conditions have to be corrected, even if the scene and its compounding objects are known. Then, the measurement correction to estimate the temperature in an outdoor context can be made and the parameters estimated by using on-site

measurements, with multi-sensor instrumentation. However, such a solution increases the instrumentation complexity and cost, the number of data to gather and store and, sometimes, it cannot be applicable at all on the experiment facility. Moreover, even with multi-sensor instrumentation, data may be lacking due to various possible issues. As a consequence, we propose to use opportunistic open data from online providers to estimate those environmental parameters.
This study aims to survey various factors that may affect measurements in outdoor infrared thermography. A particular focus is proposed on examining the influence of varying meteorological conditions and developing correction methods for these variations.

This study aims at making a survey of the different quantities that may impact the measurements in a context of outdoor infrared thermography. A particular focus on the study of varying meteorological conditions and how to correct them is proposed. First, the experimental setups are presented. Then, the proposed conversion model for computing temperature is introduced. The process of camera resectioning and the impact of environmental errors are then analyzed and discussed. Finally, the outcomes are presented and interpreted.

2. Tests sites, related instrumentations and configurations

Two tests sites have been instrumented and have gathered numerous data to exploit.

2.1. Instrumented wood house

The first one is a wood house, built under the SenseCity project of the University, and instrumented for multiple years in Paris with well-known material properties and dimensions to have a real sized and in-situ mock-up. The house is monitored by a FLIR A65 thermal infrared camera (640×512 LWIR FPA, pitch 17 µm, equipped with a 13 mm optical focal length). A weather station (VAISALA WXT 520) and a sunshine pyranometer (SPN1) gives us the total and diffuse solar radiation. A multi-sensors acquisition system is used to record and synchronize data in time. The infrared camera is placed on a mast to get a large view of the scene (see Figure 1).

2.2. Instrumented road section

The second one is an instrumented road at our laboratory in Nantes, France with a local weather station, a pyranometer a pyrgeometer and an

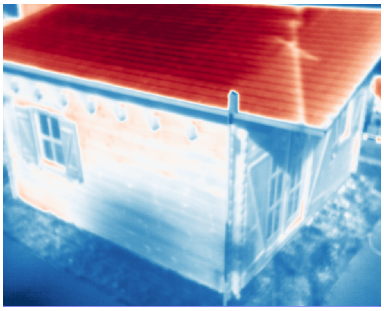

(a) Image of the wooden chalet in the infrared spectrum

(b) Image of the wooden in the visible spectrum

Figure 1: Wooden chalet instrumentation: IR image (a) and test site overview (b)

infrared camera (see Figure 2). The road section has thermocouples on the ground from which the infrared temperature estimations with the different corrections can be compared.

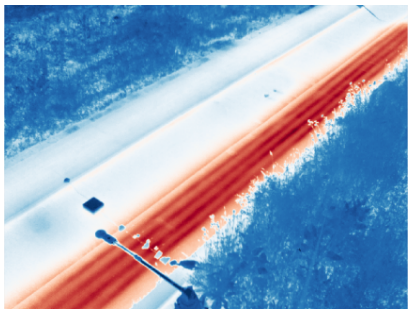

(a) Image of the concrete road in the infrared spectrum

(b) Image of the concrete road in the visible spectrum

Figure 2: Concrete road instrumentation: IR image (a) and test site overview (b)

3. Temperature computation based on a multi-sensors model

In this section, the principle and main challenges of the conversion of the received flux at camera's sensors to temperature are presented.

One of the major difficulty in *in-situ* infrared thermography temperature measurement is that the received flux depends on its surrounding environmental situation and also the thermo-optical properties of the measurement scene as described in the reference book [10] and more detailed in [5] which

are usually unknown as illustrated in Figure 3. Furthermore, the camera is placed on a mast, in this case, leading to a non-constant spatial sampling of the monitored surfaces. In such configuration, the radiation flux attenuated by the atmosphere will depend on the position of the measurement point in the scene adding even more complications to the flux to temperature conversion problem.

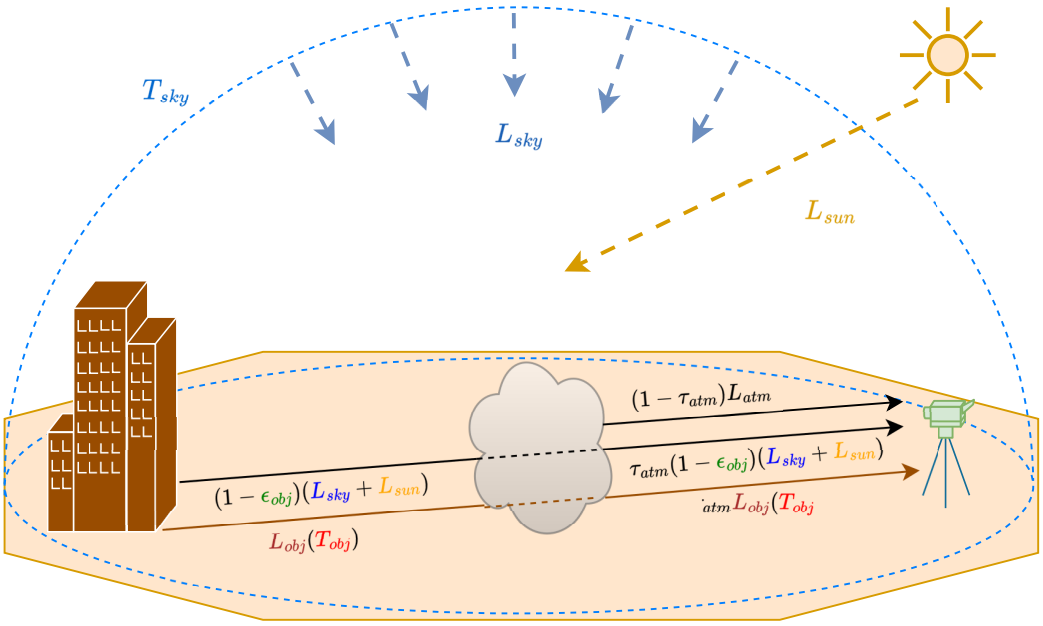

Figure 3: Radiation interactions received by cameras sensors looking at a building through a participating media.

To retrieve the flux received by the camera at each pixel L_{total}, the simplified radiometric equation that takes into account the atmospheric (L_{atm}), optic (L_{opt}) and environmental contributions from the sun (L_{sun}) and the sky (L_{sky}) is used (see Equation (1)). To first obtain an estimate of the emitted flux by the object (L_{obj}) from this measurement, it is necessary to estimate the different previous unknown quantities as well as the atmospheric transmission (τ_{atm}), optical transmission (τ_{opt}) and the emissivity of the object (ϵ_{obj}).

$$L_{\text{total}}(T) = \tau_{\text{opt}}[\tau_{\text{atm}}\left(L_{\text{obj}}(T_{\text{obj}}) + (1-\epsilon_{\text{obj}})(L_{\text{sky}}(T_{\text{sky}}) + L_{\text{sun}})\right) + (1-\tau_{\text{atm}})L_{\text{atm}}] + (1-\tau_{\text{opt}})\,L_{\text{opt}} \tag{1}$$

Once the emitted flux by the object is estimated, an RBF-function (2) is used to compute the temperature with a thermal calibration process; prior to the experiment as described in [11].

$$T_{obj} = \frac{B}{\log\left(\frac{R}{L_{obj}} - F\right)} \tag{2}$$

Finally, the overall temperature estimation through *in-situ* long-term thermal monitoring involves many parameters. The objective of the paper is to focus on the influence of those parameters in order to get an overview of the temperature estimation process bottlenecks. Then, two methods are proposed to estimate environmental parameters (*i.e.* the estimation of the emissivity and optics are done separately). A first one is to use local sensors on site, whereas the other one takes advantage of available online and open data from different providers.

4. Spatial influence

Before going further into the sensitivity of the model to its parameters, it is important to note that the position of the camera in the scene may induce effects on the obtained image. In particular, monitoring a civil engineering structure requires a large angle of view which may impose the camera to be installed on a mast or other elevating observation (for instance on top of a pylon) or under a bridge deck. However, such situation results in images with varying spatial resolutions (*e.g.* distances) and important angles between the objects and the camera (see Figure 1). The underlying consequences are non-square pixels in the real-world and varying angles values along the same plane which has an impact on the emissivity values to be considered. Moreover, practical applications may need to focus on a particular region of interest on the image to retrieve the temperature at one precise location. Knowing the geometric properties of the sensor-scene configuration on the measurement site is useful, in particular to get the view angle of the camera to the object. Retrieving the real world coordinates on the image is known as resectioning (see Figure 4). Standard spatial calibration procedures can be used and adapted from the visible by using peculiar materials pattern samples, heat sources or manual referencing (see [12] for gold-standard methods and [13] in particular for using ground control points) for this purpose.

If such process enables to recover the region of interest, it also induces a new sampling obtained by interpolation and illustrated in Figure 5. We

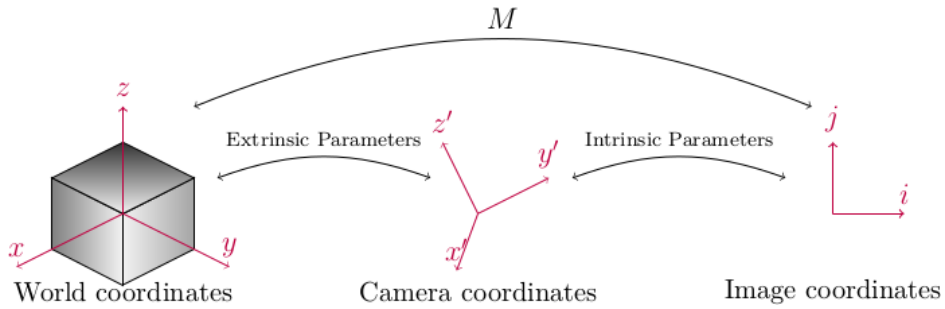

Figure 4: Resectioning principle, from world coordinates to image coordinates

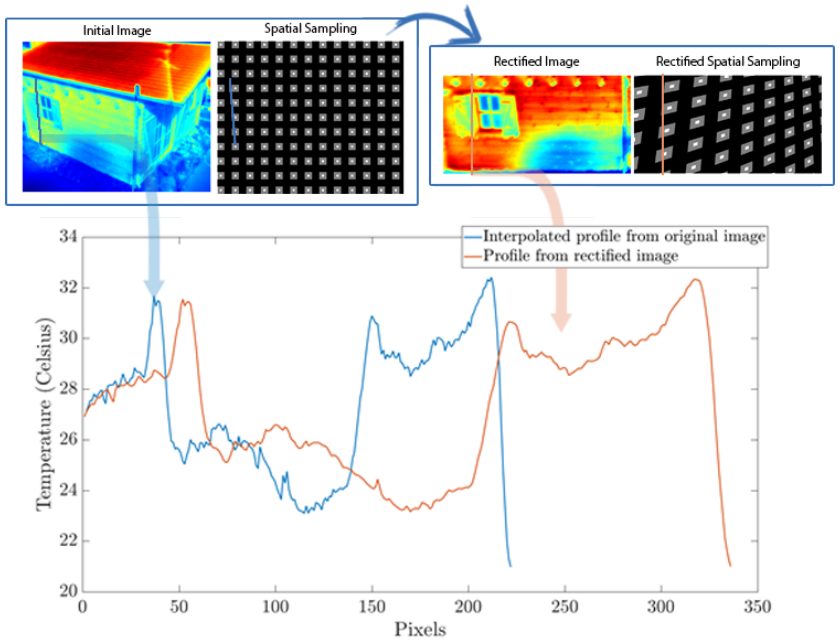

Figure 5: Illustration of sampling issues after projection

can see at the bottom of this figure the actual effect of the projection to the thermal profiles that are scaled up and smoothed due to the interpolation. Furthermore, the dilation coefficient is not constant within the image leading to a varying re-projection error induced by the interpolation depending on the considered pixel's position. Such operation can lead to a blurring of the edges and jagged artifacts.

Furthermore, the variation of distances on such scenes induce a mixed pixel effect, where one pixel is not the representation of a particular object's surface but a mixture of materials. As a consequence, the material properties are not equivalent from the world coordinates to the image one, due to the induced spatial integration. One solution is to perform sub-pixel analysis, by using histogram analysis methods, data fusion, oversampling, *etc.* [14]. Such concern is particularly studied in the remote sensing field as in [15] where a simulation is used to demonstrate the impact of having mixed pixels on land surface phenology or even [16] that demonstrates the complexity of having such phenomenon in land data classification.

5. Conversion model sensitivity to parameters

In addition to spatial considerations, the lack of knowledge about the observed surfaces may affect the temperature estimation based on infrared measurements. In particular, the emissivity estimation will have an important impact on the final temperature estimation. Moreover, various meteorological and environmental factors will affect the temperature estimation based on infrared measurements [17]. A review of the impact of the different errors made for the temperature estimation based on the model and presented in Equation (1) is done in this part. Different analysis of sensitivity have been previously done in the literature, by comparing sensitivity between shortwave and longwave measurements [18], by performing the analysis on dual-band measurements systems [19] or for high temperature measurements [20] for instance. Moreover, reference book [21], the book chapter [22] and [23] provide a comprehensive analytical analysis of the errors made on infrared measurements while [24] provides a full list of uncertainties budgets for the calibration of radiation thermometers. Those analyses are extended to the case of the *in-situ* model presented previously and focus on the emissivity, environment temperature and atmospheric transmission effects. By considering that the object's temperature and emissivity are independent:

$$\begin{cases} \frac{\partial L_{total}}{\partial \epsilon_{obj}} & = \tau_{atm}\tau_{opt}\left(L_{obj} - L_{sky}\right) \\ \frac{\partial L_{total}}{\partial T_{sky}} & = \left(1-\epsilon_{obj}\right)\tau_{atm}\tau_{opt}\frac{\partial L_{sky}}{T_{sky}} = \left(1-\epsilon_{obj}\right)\tau_{atm}\tau_{opt}\frac{RBe^{B/T_{sky}}}{T_{sky}^2(e^{B/T_{sky}}+C)^2} \\ \frac{\partial L_{total}}{\partial \tau_{atm}} & = \epsilon_{obj}\tau_{opt}L_{obj} + (1-\epsilon_{obj})\tau_{opt}L_{sky} - \tau_{opt}L_{atm} \end{cases} \quad (3)$$

Those equations will be used in the following in order to observe the impact of the different model's parameters to the temperature retrieval while neglecting the influence of the optics transmission τ_{opt}.

5.1. Model sensitivity to emissivity

Emissivity measurements have been made on the wood house (see section 2.1) in order to get an emissivity map, represented in Figure 6. The system used for measurements was a portable emissometer developed at CERTES [25]. Table 1 shows the associated emissivity measurements.

Material	Color	Emissivity
Wood wall (west)	Blue	0.95
Wood wall (east)	Yellow	0.90
Grass	Green	0.95
Sidewalk	Red	0.89
Tar	Grey	0.95
Roof	Purple	0.92

Table 1: Emissivity measurements values in the $8\mu m - 14\mu m$ band.

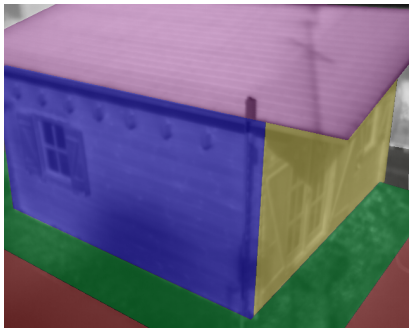

Figure 6: Emissivity map for the wood house, colors represents one particular emissivity measurement

Figure 7 shows the effect of adjusting the emissivity to a particular material. In this case, the comparison can only be made relatively due to the lack of ground truth temperature measurements at the surface of the different materials.

However, one can see that adjusting the emissivity will refine the temperature estimation. In fact, in this example, a fair candidate for a constant emissivity value over the entire image can be 0.93 which is the average emissivity value is with a standard deviation of 0.025 (derived from Table 1 and Figure 6). When neglecting all the other effects but the emissivity value,

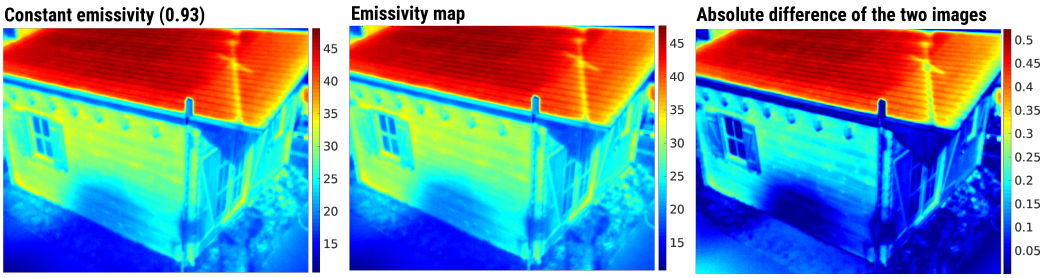

Figure 7: Effect of adjusting the emissivity in temperature estimation for different material compared to a constant emissivity

choosing a coarse emissivity map instead of a constant emissivity value on the image leads to, at most, 0.5 K difference for a given thermal equilibrium at a fixed time of observation (see last image of Figure 7). This example also demonstrates that the error in the temperature estimate is not constant across the pixels of the image. Furthermore, emissivity will be a factor in all parameters in Equation 1 and will, therefore, play an essential role in temperature estimation. However, in this paper, the focus is made on environmental parameters. Nevertheless, more details on the error induced by emissivity, along with sky temperature and atmospheric transmission, are presented in the next two sections.

5.2. Model sensitivity to sky temperature and atmospheric transmission

The sky temperature (T_{sky}) is an important concept when doing radiative balances. It represents the apparent effective temperature of the sky assumed to behave like a blackbody. It is therefore different from the ambient air temperature and can be lower, particularly under clear sky conditions. Such quantity will have an impact on the final temperature estimation ($\tilde{T}_{obj}$), as shown in Figure 8 where the difference between the estimated sky temperature ($\tilde{T}_{sky}$) is compared to the difference made on the estimated object temperature, for different values of T_{obj} and T_{sky} . The R, B and F values used in the model to compute this figure are derived from a thermal calibration. One can note that those coefficients are only valid for a limited range of object temperature (283.15 K - 343.15 K in this case) and could expect some more important error out of this range. Figure 8 compares the differences between the actual object temperature and the estimated one by using estimates on T_{sky} ($\tilde{T}_{sky}$) and ϵ_{obj} ($\tilde{\epsilon}_{obj}$).

Finally, Figure 9 illustrates the accumulation of errors made on the atmo-

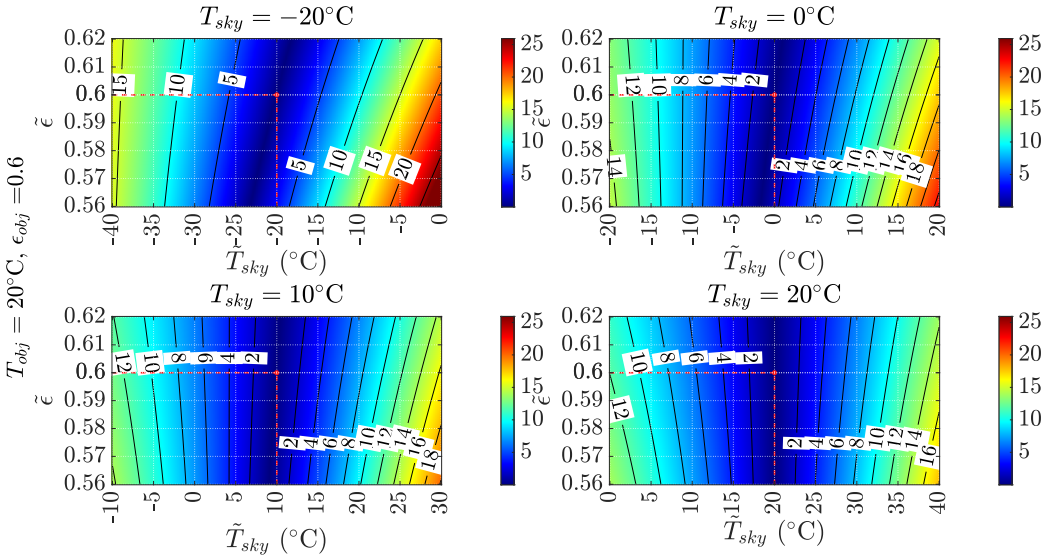

Figure 8: Difference between true object temperature and estimated one depending on the error made on the sky temperature and emissivity. In this case, the true object is at 20 °C and its emissivity is 0.93.
How to read: on the left the true object's temperature and emissivity. A point on the image represents the difference between the true object temperature and the estimated one with $\tilde{T}_{sky}$ (x-axis) and $\tilde{\epsilon}_{obj}$ (y-axis) values. The images represent different environmental temperatures values.

spheric transmission and on the emissivity to the estimation of temperature. Similarly to Figure 8 and based on Equation (3), the map of the differences between the estimated temperature and the expected one can be made by considering the error made on the atmospheric transmission.

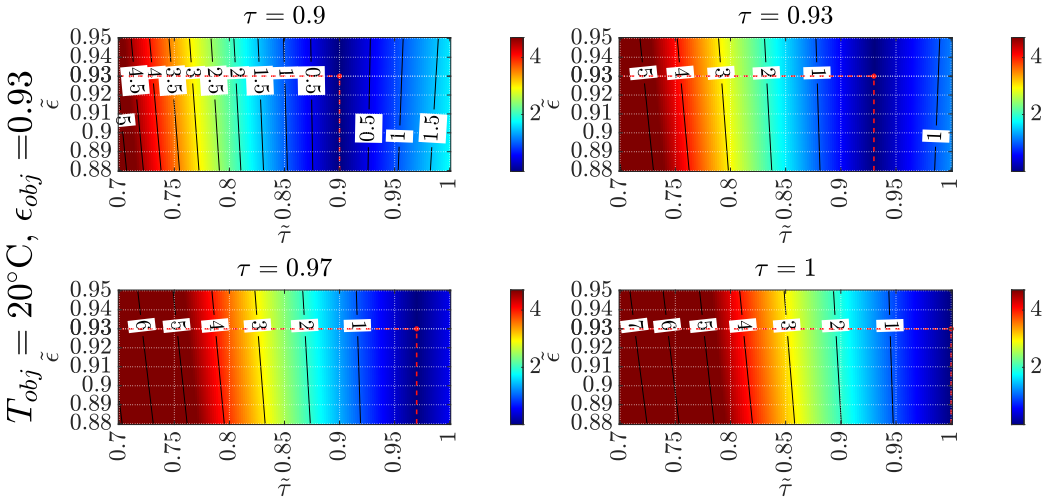

Figure 9: Difference between true object temperature and estimated one depending on the error made on the atmospheric transmission and emissivity. Here is the difference map for an object temperature of 20 °C and emissivity of 0.93.
How to read: on the left the true object's temperature and emissivity. A point on the image represents the difference between the true object temperature and the estimated one with $\tilde{\tau}_{atm}$ (x-axis) and $\tilde{\epsilon}_{obj}$ (y-axis) values. The images represent different atmospheric transmissions values.

Moreover, the atmospheric transmission is usually approximated by using the ambient temperature, relative humidity, and involved distance at operating wavelength[26]. In particular, when dealing with infrastructures monitoring applications, great distances differences may occur due to large field of views (*e.g.* during the monitoring of a bridge). In such case, a spatial calibration is necessary to compute a distance map and take into account those distances. As for example, Figure 10 shows the effect of the distance to the atmospheric transmission in the 7.5 µm to 13 µm band and the need for considering the distances due to the camera view projection within the image. As shown in this figure, considering the same distance between the observed surface and the camera may lead to inaccuracies.

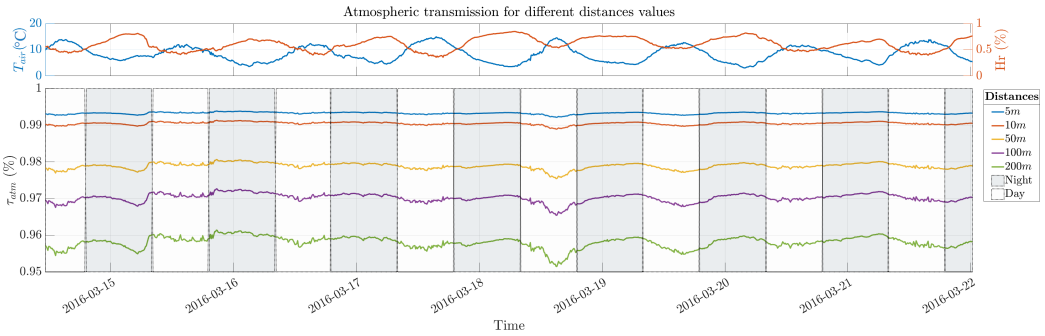

Figure 10: Different distance values for the atmospheric transmission, through time.

5.3. Sun's irradiance considerations

The sun's irradiance will also have an impact on the final temperature estimation. In fact, depending on the emissivity of the observed object, the irradiance at camera's sensor will contain the sun's reflected contribution, both specular and diffuse. In the case of the LWIR (7.5 µm to 13 µm), even though the sun contribution may be small compared to the NIR, SWIR and MWIR bands, it stills represents a source of error in the conversion process. In particular for low object's temperatures as illustrated in Figure 11, we can see that the direct sun irradiance contribution can be responsible for up-to 3% of the object's emittance, leading to incorrect temperature estimation if not considered. In the case of SWIR-MWIR band the sun contribution should not be neglected, in particular when observing surfaces with low temperatures (Figure 12).

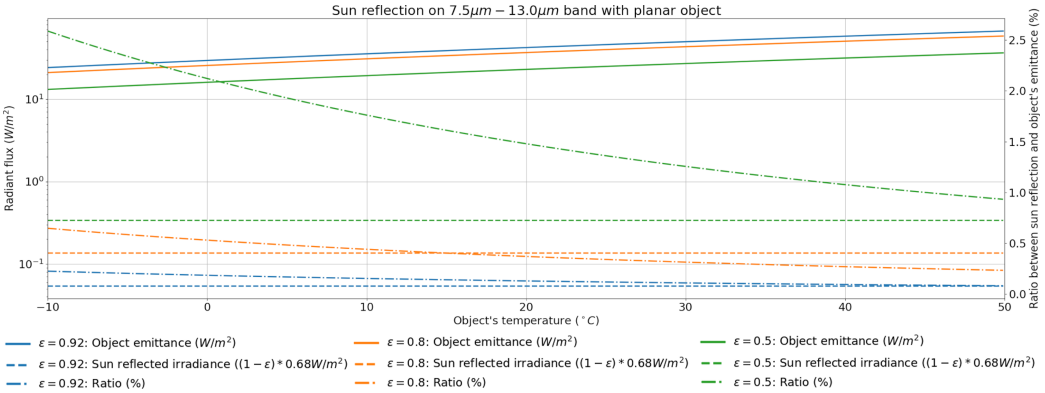

Figure 11: Sun irradiance reflection on the 7.5 µm to 13 µm band for a normal object and different emissivity values

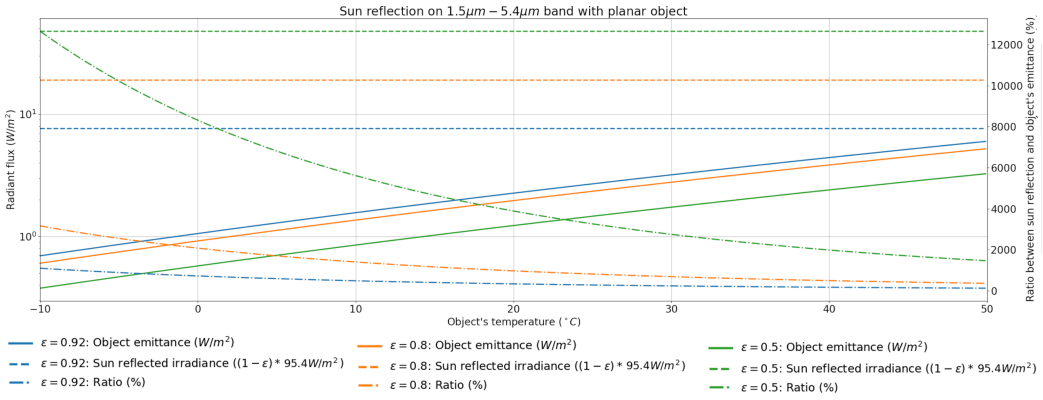

Figure 12: Sun irradiance reflection on the 1.5 µm to 5.4 µm band for a normal object and different emissivity values

5.4. Discussion

The main parameters that will have an impact on the final temperature estimate in an outdoor infrared thermography monitoring system have been presented in this section. It is important to note that the final estimation depends not only on the error in one parameter but also on the combined errors in each parameter estimation. Additionally, the conditions of operation and the properties of the material influence the final error in the temperature estimate. This is particularly illustrated in Figure 8 and Figure 9. Consequently, in the next section, we propose two methods to estimate these environmental parameters under operational conditions using local sensor data or opportunistic (online) data. Finally, a comparison between what is measured with the different corrections methods and without any correction is given in Section 6.6.

6. Parameters Estimation

Previous sections have enlightened that to achieve quantitative thermography, one must consider the global radiative heat balance at the sensor level and be able to estimate the different parameters of the equation. Then, the measurement correction to estimate the temperature in an outdoor context can be made. One way to estimate the involved parameters is to use on-site measurements, with a multi-sensors instrumentation. However, such a solution increases the instrumentation complexity and cost, the number of data to gather and store and, sometimes, it cannot be applicable at all on the

experiment facility. Moreover, even with a multi-sensors instrumentation, data may be lacking due to various possible issues. In this part, the focus is made on the practical consideration of those parameters, in operating conditions. Different means, at different scales, to estimate those parameters are proposed and compared.

6.1. Emissivity considerations

Taking into account the emissivity in such measurements is a challenging task that may result to important uncertainties in the temperature estimation process, as illustrated in Figure 8. Emissivity measurements or tables could be used, notably by using a Building Information Model (BIM) giving detailed data about materials used in the construction. However, such data may not be available, and tables data may not reflect the materials' reality since the emissivity relies on the state of the surface [21].

Another possibility is to use the physical equations, which are an ill-posed problem known as the temperature and emissivity separation (TES) problem [10]. Even though different methods have been developed (see a review from [27] or [28] for land surface temperature estimation), using Bayesian inference with Monte-Carlo Markov Chains (MCMC) [29] or Kalman filtering with [30] and [31], Maximum Entropy estimator [32] , or even neural networks [33], the TES problem is still challenging and often addressed in the remote sensing field. In fact, the developed methods rely on particular application hypothesis, on a specific materials' database (for neural network training for instance [34]) or are computationally intensive as for the MCMC method [29]. Recent researches, based on Bayesian methods have been proposed to tackle such challenge in the particular context of outdoor long term monitoring, but more evaluations need to be made[35].

6.2. Environmental Parameters Estimation

To estimate the environmental parameters, we propose and compare three methods: local measurements from the instrumented road (see Section 2), existing sensor networks with Meteorological Aerodrome Report (METAR) data and open source online satellite data from the European Copernicus program. Since some data may not be available from all the different sources, we also propose literature correlations or methods to be used to deduct those quantities.

6.2.1. Meteorological Aerodrome Report (METAR)

METAR is a normalized format to create weather reports, based on permanent weather observation stations or airports, that are generated periodically (usually once an hour). The methodology we propose is to download data from the nearest available METAR station.

6.2.2. Copernicus Climate Data Store (CDS)

The Climate Data Store (CDS) is part of the European program Copernicus aiming at collecting and providing edge-cutting and updated continuous data on Earth's state. The CDS provides a single point access to many European datasets including observations, reanalysis and forecasts. For post-processing temperature computation, we propose to use the reanalysis dataset and particularly ERA5-land dataset [36].

6.3. Sky temperature

One can use the measurements made *in-situ* to get the sky temperature. As for example, in Figure 13, the ground truth temperature obtained from thermocouples data is compared to the temperatures estimated with and without sky correction on a different test site. In the case of the sky correction, the sky temperature is derived from a pyrgeometer data whereas a constant sky temperature is taken in the other case. Figure 13 shows that taking into account the sky temperature from local measurements gives a better estimate of the object temperature. In this particular example, the estimation of the temperature with and without the sky temperature correction is compared to thermocouples measurements at the surface of a concrete pavement structure. The sky correction reduces in average the difference between the thermocouples measurements and the estimated temperature from infrared data.

Another possibility is to use correlations from measured air temperature to estimate the sky temperature. Such correlations can be found in the literature [37]. Figure 14 shows the effect of the Swinbanks correlation for two different periods: in december and august. Moreover, one can see that the sky temperature derived from the correlation will have an impact of the same magnitude's order as if using *in-situ* measurements.

If local measurement data are not available, the correlation formula can be used from various online data providers, as introduced previously. Figure 15 shows the sky temperature derived from the different providers. Even if differences exists in term of sky temperature, it represents a small quantity

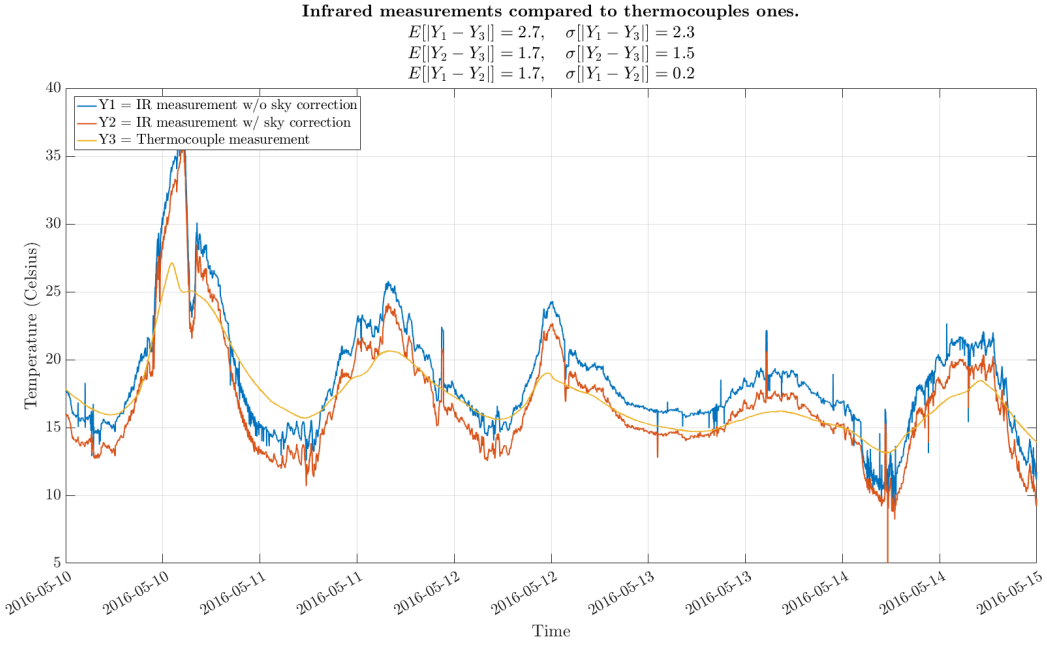

Figure 13: Comparison of ground truth temperature values to temperature estimation with and without sky correction

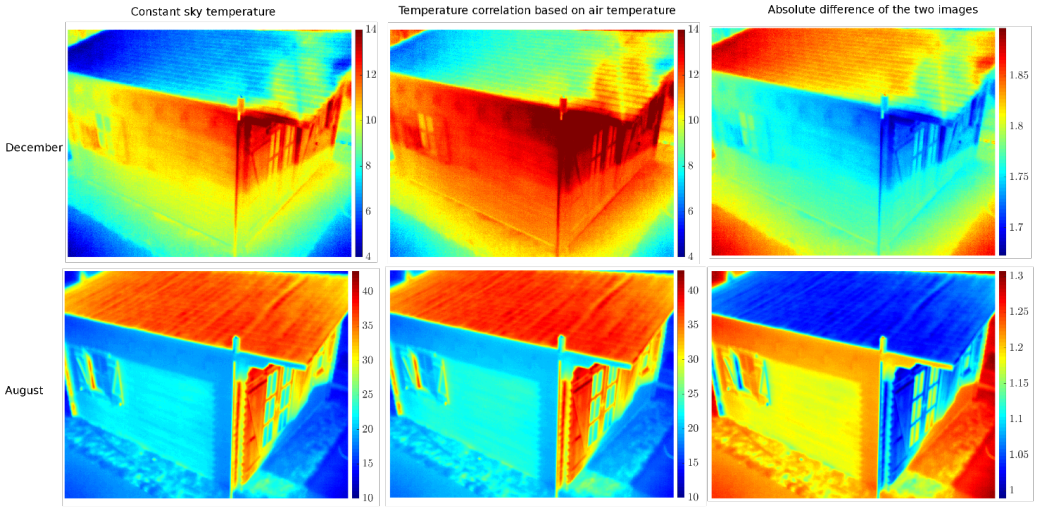

Figure 14: Effect of using a correlation for the sky temperature based on the air temperature measurement

of thermal radiation, regarding the involved temperatures. Therefore, it is always possible to enrich the radiative model conversion thanks to online and open data.

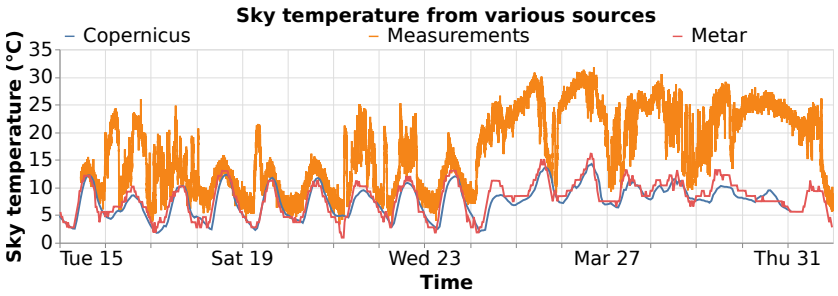

Figure 15: Sky temperature derived from different sources of air temperature

6.4. Atmospheric Transmission

Similarly, atmospheric transmission can also be obtained using different sources. Figures 16 and 17 show the air temperature and relative humidity from the various sources, respectively.

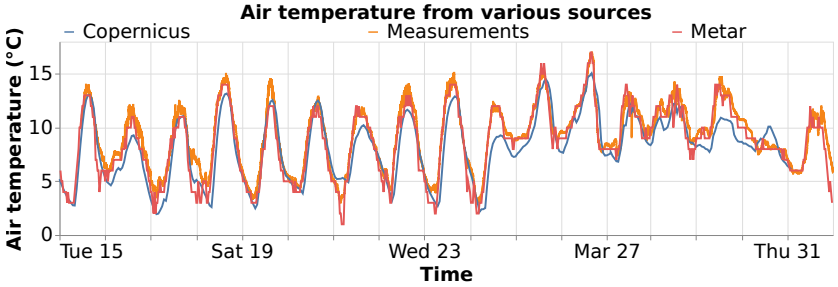

Figure 16: Air temperature obtained from different sources

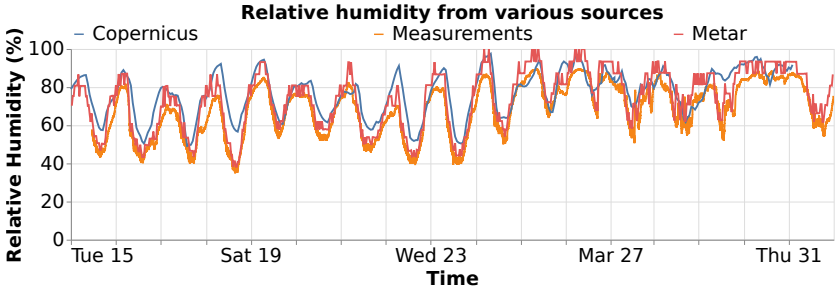

Figure 17: Relative humidity obtained from different sources

Finally, the estimated atmospheric transmission coefficient is shown in Figure 18, using the previous quantities from the different data providers.

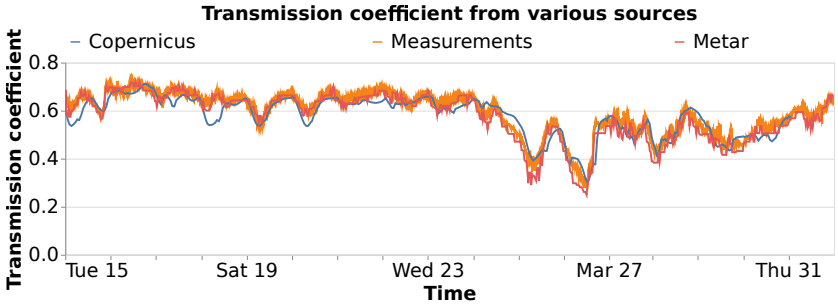

Figure 18: Atmospheric transmission derived from different sources

6.5. Sun irradiance

The sun irradiance is not often present in METAR data. For other providers, such as Copernicus, it is integrated over the whole spectrum, leading to errors on the quantities to be considered. Figure 19 shows the SMARTS2 [38] irradiance's simulation compared to a local pyranometer measure in the SWIR band.

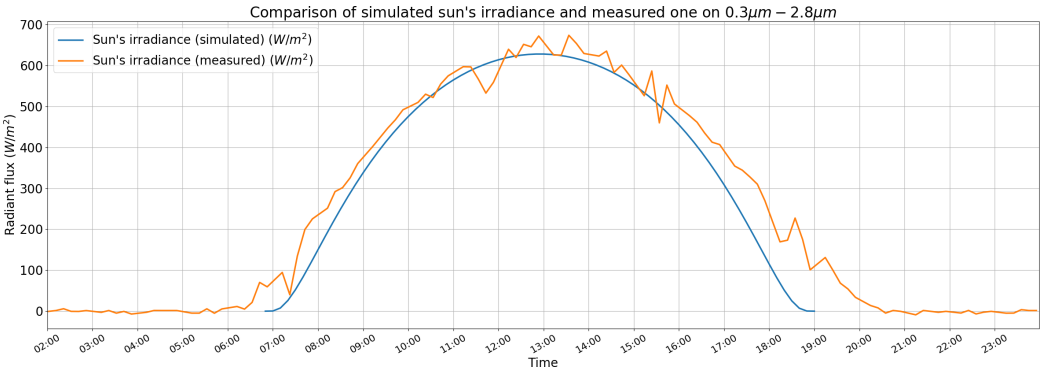

Figure 19: Comparison of sun's irradiance measured and simulated on may 5th in the 0.3 µm to 2.8 µm band

Other models can be found in the literature and can help for getting an approximation of the sun irradiance on the considered band.

6.6. Discussion

A review of the different parameters that may affect the temperature estimation has been made. Temperature estimation based on *in-situ* infrared thermography measurements needs to consider the geometry of the scene and the environmental parameters to get a better estimate. When local data are not available, it is possible to find online open data thanks to meteorological reports or forecasts. Figure 20 shows an example of the amount of data that can be gathered during a long-term experiment with missing data in red due to various experiment issues (sensor failure, current shortage *etc.*). This study showed that even if those measurements are missing, it is still possible to estimate those data thanks to open access online data to enable the usage of a refined model.

Finally, a comparison of the estimated temperature with the infrared camera and a thermocouple at ground has been performed and results are shown in Figure 21. Even if the thermocouple measurement cannot be considered

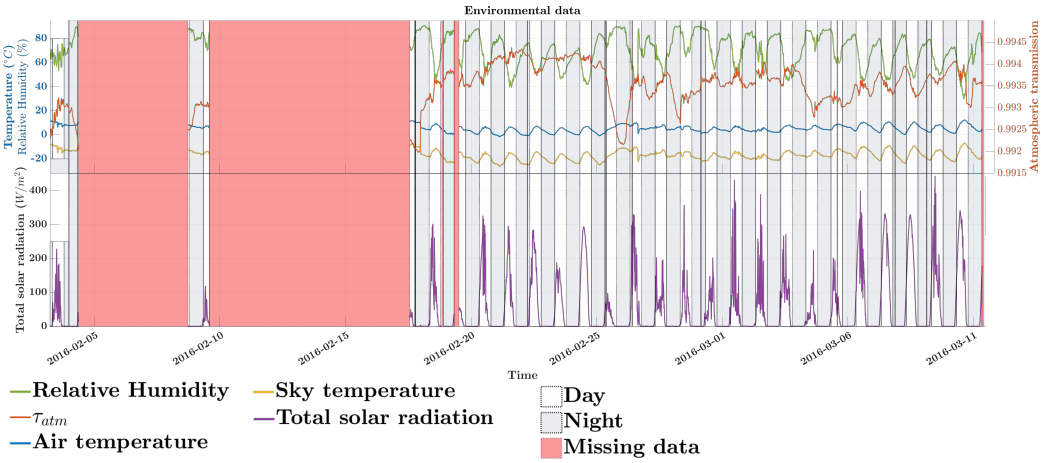

Figure 20: A set of environmental data for long-term thermal monitoring

as a ground truth, it is still a fair temperature reference. In this figure, it can be seen that on this period of interest, any consideration of environmental parameters from any provider will make the estimation closer to the thermocouple measure. In particular, on-site measurements provide, on average, the closest temperature estimation to the thermocouple.

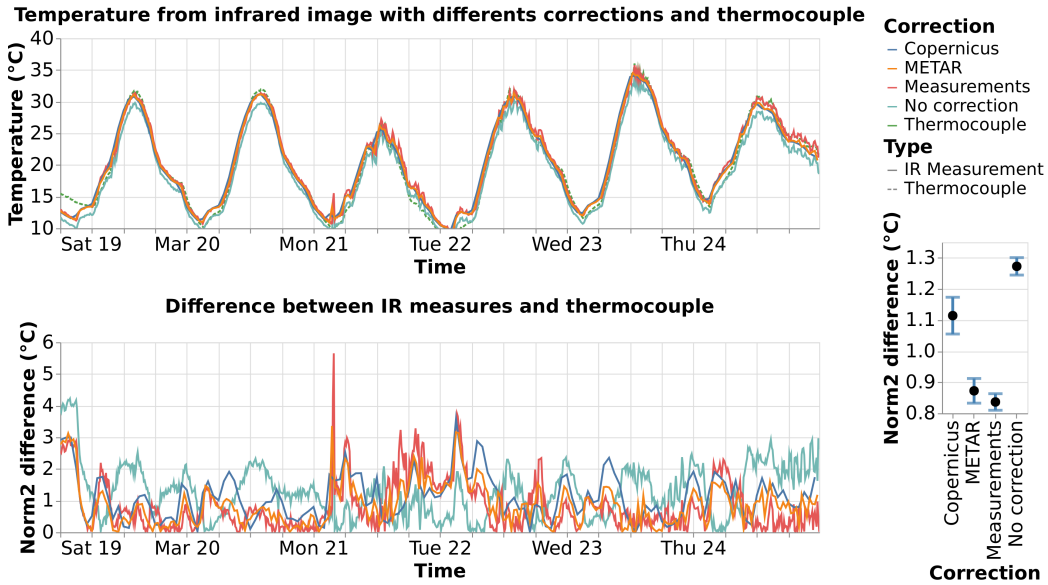

Figure 21: Comparison between infrared temperature estimation (solid) and the corresponding thermocouple at ground (dashed). Infrared temperature estimations are computed without and with different types of environmental corrections by using parameters from on-site measurements, METAR and Copernicus CDS (**top**). The absolute difference with the thermocouple is also represented (**bottom-left**) as well as the average on the period of interest (**bottom-right**).

Finally, more investigations need to be made for particular weather conditions such as snow and rain for instance, which were not observed during the studied period. Hydrometeors will have an important impact on the flux received at camera's sensors. Weather variations will produce measurements that are difficult to exploit for accurate temperature estimation (see Figure 22). This may not lead to accurate temperature measurements. However, such effect could be compensated by using a black-body source and perform automatic thermal calibration in case of rain or using adequate radiative transmission model (for instance in case of fog [39]).

7. Conclusion

A study of the different parameters that create bias in long term thermal monitoring of structures by infrared thermography has been conducted. To achieve in-situ accurate temperature estimation from those measurements, one need to take into account the environmental parameters, the geometry

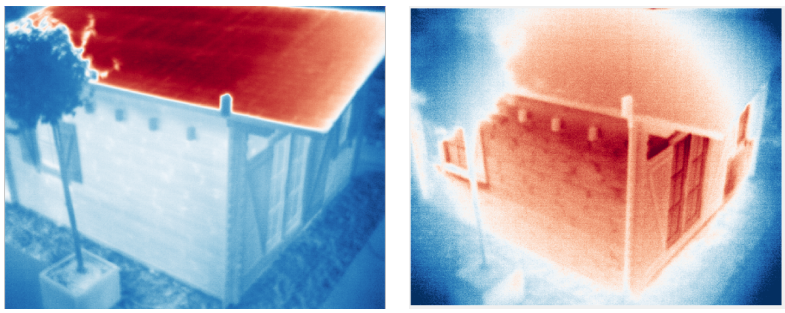

(a) Dry situation (b) Raining and optic issues

Figure 22: IR image view: in dry environment (a), rain with optic issues (b)

of the scene and the characteristics of the observed materials. Using local and coupled measurements with those infrared data enables the temperature estimation to be more accurate.

The spatial calibration presented in this study makes the extraction of region of interest possible. One other possibility is to use stereo-vision [40] to get a more accurate calibration and in particular to retrieve the depth in the image. Further investigation is required to apply computer vision algorithm for infrared images, since the infrared sensors responses have a different response than in the visible spectrum. In any case, after resectioning, the resulting signal should be considered with caution since the sampling is not uniform. Moreover, the pixels of the image do not represent the same area in the real-world due to the perspective projection. Furthermore, one should also consider the "mixed pixel effect" due to the spatial resolution for accurate infrared measurements. In fact, considering that one given pixel is homogeneous can be discussed.

After presenting a sensitivity study on the environmental parameters and emissivity to quantify their effects on temperature estimation, we focused our work on environmental parameters estimation. Moreover, it has been shown that different meteorological sources could be used similarly to enrich the monitoring's informations. Finally, taking into account the actual sky temperature in our model as well as mapping the emissivity to the image materials enabled us to reduce the difference between the temperature estimation and the expected surface temperature. Estimating the sky temperature by a correlation gives satisfying results in a first approximation but should be tested for limit cases. However, hydrometeors' influence and optics' aberrations are not incorporated in our conversion model from digital

levels to temperature yet. One of the prospects is to use the meteorological data coupled with a deep learning algorithm to compensate those effects. A second perspective is to use a Bayesian model to further consider the joint estimation of the emissivity and the temperature.

8. Acknowledgements

Authors wish to thank for their support: Sense-City Facility of Excellence of ANRs Future Investment Program, French Region Bretagne, and Antoine Crinière and Jean-Luc Manceau for their technical support during experiments.

References

[1] S. Pereira, F. Magalhães, E. Caetano, Á. Cunha, T. Toullier, J. Dumoulin, Dynamic Monitoring of a Cable-Stayed Bridge: Monitoring System and First Results, in: EWSHM 2022 - 10th European Workshop on Structural Health Monitoring, European Workshop on Structural Health Monitoring, Palermo, Italy, 2022, pp. 1–9. doi:10.1007/978-3-031-07258-1_4.
URL https://inria.hal.science/hal-03895778

[2] T. Toullier, A. Bouché, J. Dumoulin, Design and study of an instrumentation and software for permanent monitoring of a cable-stayed bridge, in: LATAM-SHM 2023 - 1st Latin American Workshop on Structural Health Monitoring, Proceedings, Cartagena de Indias, Colombia, 2023, pp. 1–8.
URL https://inria.hal.science/hal-04303006

[3] L. Yang, Y. Li, Simple correction methods of infrared thermography for building exterior surfaces, International Journal of Ventilation 9 (3) (2016) 261–272. doi:10.1080/14733315.2010.11683885.

[4] G. C. E. Grinzato, P. Bison, Moisture map by ir thermography, Journal of Modern Optics 57 (18) (2010) 1770–1778. doi:10.1080/09500341003731597.

[5] J. Dumoulin, A. Crinière, R. Averty, The detection and thermal characterization of the inner structure of the 'Musmeci' bridge deck by infrared

thermography monitoring, Journal of Geophysics and Engineering 10 (6) (2013) 064003. doi:10.1088/1742-2132/10/6/064003.

[6] N. Lalanne, J.-C. Krapez, C. L. Niliot, X. Briottet, J. Pierro, L. Labarre, Development and validation of a numerical tool for simulating the surface temperature field and the infrared radiance rendering in an urban scene, Quantitative InfraRed Thermography Journal 12 (2) (2015) 196–218. doi:10.1080/17686733.2015.1066134.

[7] A. Crinière, J. Dumoulin, L. Mevel, Management of local multi-sensors applied to SHM and long-term infrared monitoring: Cloud2IR implementation, Quantitative InfraRed Thermography Journal 0 (0) (2018) 1–19. doi:10.1080/17686733.2018.1519752.

[8] X.-B. Sui, Q. Chen, G.-H. Gu, N. Liu, Research on the response model of microbolometer, Chinese Physics B - CHIN PHYS B 19 (10 2010). doi:10.1088/1674-1056/19/10/108702.

[9] C. Ringqvist, Flir project-modeling noise in bolometer signal, 2018. URL `https://api.semanticscholar.org/CorpusID:221710208`

[10] J. Howell, R. Siegel, M. Pinar, Thermal Radiation Heat Transfer., 5th Edition, CRC Press, 2010.

[11] T. Toullier, J. Dumoulin, L. Mevel, Étude comparative de deux approches, thermocouples intégrés et thermographie infrarouge, pour la surveillance thermique d'une infrastructure de transport, in: 25eme Congrès Français de Thermique, 2017.

[12] E. K. P. Chong, S. H. Zak, An Introduction to Optimization, 4th Edition, Wiley-Blackwell, Hoboken, New Jersey, 2013.

[13] J. Pérez Muñoz, C. Ortiz Alarcón, A. Osorio, C. Mejía, R. Medina, Environmental applications of camera images calibrated by means of the Levenberg–Marquardt method, Computers & Geosciences 51 (2013) 74–82. doi:10.1016/j.cageo.2012.07.016.

[14] H. Jones, X. Sirault, Scaling of Thermal Images at Different Spatial Resolution: The Mixed Pixel Problem, Agronomy 4 (3) (2014) 380–396.

[15] X. Chen, D. Wang, J. Chen, C. Wang, M. Shen, The Mixed Pixel Effect in Land Surface Phenology: A Simulation Study, Remote Sensing of Environment 211 (2018) 338–344.

[16] A. L. Choodarathnakara, D. T. A. Kumar, D. S. Koliwad, D. C. G. Patil, Mixed Pixels: A Challenge in Remote Sensing Data Classification for Improving Performance 1 (9) 11.

[17] S. Van De Vijver, M. Steeman, N. Van Den Bossche, K. Carbonez, A. Janssens, The influence of environmental parameters on the thermographic analysis of the building envelope, in: 12th International Conference on Quantitative InfraRed Thermography (QIRT 2014), 2014.

[18] K. Chrzanowski, Comparison of shortwave and longwave measuring thermal-imaging systems, Applied optics 34 (16) (1995) 2888–2897.

[19] K. Chrzanowski, Influence of measurement conditions and system parameters on accuracy of remote temperature measurement with dual-spectral IR systems, Infrared Physics & Technology (37) (1996) 295–306.

[20] M. Pfänder, E. Lüpfert, P. Heller, Pyrometric Temperature Measurements on Solar Thermal High Temperature Receivers, Journal of Solar Energy Engineering 128 (3) (2006) 285. doi:10.1115/1.2210499.

[21] G. Gaussorgues, S. Chomet, Infrared Thermography, Springer Science & Business Media, 1993.

[22] J.-C. Krapez, Radiative Measurements of Temperature, in: Thermal Measurements and Inverse Techniques, Heat Transfer, CRC Press, Boca Raton, FL, 2011, oCLC: ocn587104377.

[23] W. Minkina, S. Dudzik, Infrared Thermography: Errors and Uncertainties, John Wiley & Sons, 2009.

[24] P. Saunders, J. Fischer, M. Sadli, M. Battuello, C. W. Park, Z. Yuan, H. Yoon, W. Li, E. van der Ham, F. Sakuma, J. Ishii, M. Ballico, G. Machin, N. Fox, J. Hollandt, M. Matveyev, P. Bloembergen, S. Ugur, Uncertainty Budgets for Calibration of Radiation Thermometers below the Silver Point, International Journal of Thermophysics 29 (3) (2008) 1066–1083. doi:10.1007/s10765-008-0385-1.

[25] J.-P. Monchau, M. Marchetti, L. Ibos, J. Dumoulin, V. Feuillet, Y. Candau, Infrared emissivity measurements of building and civil engineering materials: A new device for measuring emissivity, International Journal of Thermophysics 35 (2014) 1817–1831. doi:10.1007/s10765-013-1442-y.

[26] W. Minkina, D. Klecha, Atmospheric transmission coefficient modelling in the infrared for thermovision measurements, Journal of Sensors and Sensor Systems 5 (01 2016). doi:10.5194/jsss-5-17-2016.

[27] S. B. A. Rolim, A. Grondona, C. L. Hackmann, C. Rocha, A Review of Temperature and Emissivity Retrieval Methods: Applications and Restrictions, American Journal of Environmental Engineering 6 (2016) 119–128.

[28] Z.-L. Li, B.-H. Tang, H. Wu, H. Ren, G. Yan, Z. Wan, I. F. Trigo, J. A. Sobrino, Satellite-derived land surface temperature: Current status and perspectives, Remote Sensing of Environment 131 (2013) 14–37. doi:10.1016/j.rse.2012.12.008.

[29] J. N. Ash, J. Meola, Temperature-emissivity separation for LWIR sensing using MCMC, in: Algorithms and Technologies for Multispectral, Hyperspectral, and Ultraspectral Imagery XXII, Vol. 9840, International Society for Optics and Photonics, 2016, p. 98401O. doi:10.1117/12.2223263.

[30] G. Masiello, C. Serio, I. De Feis, M. Amoroso, S. Venafra, I. F. Trigo, P. Watts, Kalman filter physical retrieval of surface emissivity and temperature from geostationary infrared radiances, Atmospheric Measurement Techniques 6 (12) (2013) 3613–3634. doi:10.5194/amt-6-3613-2013.

[31] M. Pivovarník, S. J. S. Khalsa, J. C. Jiménez-Muñoz, F. Zemek, Improved Temperature and Emissivity Separation Algorithm for Multispectral and Hyperspectral Sensors, IEEE Transactions on Geoscience and Remote Sensing 55 (4) (2017) 1944–1953. doi:10.1109/TGRS.2016.2631508.

[32] A. Barducci, D. Guzzi, C. Lastri, P. Marcoionni, V. Nardino, I. Pippi, Emissivity and Temperature Assessment Using a Maximum Entropy Estimator: Structure and Performance of the MaxEnTES Algorithm,

IEEE Transactions on Geoscience and Remote Sensing 53 (2) (2015) 738–751. doi:10.1109/TGRS.2014.2327218.

[33] N. Wang, Z.-L. Li, B.-H. Tang, F. Zeng, C. Li, Retrieval of atmospheric and land surface parameters from satellite-based thermal infrared hyperspectral data using a neural network technique, International Journal of Remote Sensing 34 (9-10) (2013) 3485–3502. doi:10.1080/01431161.2012.716536.

[34] J. F. Mas, J. J. Flores, The application of artificial neural networks to the analysis of remotely sensed data, International Journal of Remote Sensing 29 (3) (2008) 617–663. doi:10.1080/01431160701352154.

[35] T. Toullier, J. Dumoulin, L. Mevel, A Kriging-based Interacting Particle Kalman Filter for the simultaneous estimation of temperature and emissivity in Infra-Red imaging, in: IFAC 2020 – 21st IFAC World Congress, Berlin, Germany, 2020.
URL `https://inria.hal.science/hal-02940184`

[36] J. Muñoz Sabater, ERA5-Land hourly data from 1950 to present. Copernicus Climate Change Service (C3S) Climate Data Store (CDS), `https://doi.org/10.24381/cds.e2161bac`, [Online; accessed 01-November-2023] (2019). doi:10.24381/cds.e2161bac.

[37] L. Adelard, F. Pignolet-Tardan, T. Mara, P. Lauret, F. Garde, H. Boyer, Sky temperature modelisation and applications in building simulation, Renewable Energy 15 (1998) 418–430. doi:10.1016/s0960-1481(98)00198-0.

[38] C. Gueymard, Simple Model for the Atmospheric Radiative Transfer of Sunshine (SMARTS2) Algorithms and Performance Assessment, 1995.

[39] J. Dumoulin, V. Boucher, Infrared thermography system for transport infrastructures survey with inline local atmospheric parameter measurements and offline model for radiation attenuation evaluations, Journal of Applied Remote Sensing 8 (1) (2014) 084978–084978.

[40] R. I. Hartley, A. Zisserman, Multiple View Geometry in Computer Vision, 2nd Edition, Cambridge University Press, ISBN: 0521540518, 2004.